Chalcogenide Letters Vol. 20, No. 7, July 2023, p. 459 - 467

Optical and magnetic characteristics of $BaTi_{1-x}Co_xO_3$: A first-principles study

M. K. Butt[a], S. Saleem[a], F. F. Al-Harbi[b], S. Atta[a], M. Ishfaq[a], F. S. Al Juman[c], M. Yaseen[a,*]
[a]*Spin-Optoelectronics and Ferro-Thermoelectric (SOFT) Materials and Devices Laboratory, Department of Physics, University of Agriculture, Faisalabad 38040, Pakistan*
[b]*Department of Physics, College of Sciences, Princess Nourah bint Abdulrahman University, P. O. Box 84428, Riyadh 11671, Saudi Arabia*
[c]*Department of Physics - College of Science and Arts in Sarat Abidah - King Khalid University, Abha, Saudi Arabia*

The full potential linearized augmented plane wave (FP-LAPW) approach based on the density functional theory (DFT) is employed to know the effect of Co doping on the electronic, optical, and magnetic characteristics of $BaTi_{1-x}Co_xO_3$ at x= 8.33%, 16.66%, 25%, and 50%. The computed spin-polarized electronic band structure (BS) and the density of states (DOS) elucidate that the $BaTi_{1-x}Co_xO_3$ compound has a ferromagnetic semiconductor behavior at all doping concentrations. The results indicate that the magnetic moment in $BaTi_{1-x}Co_xO_3$ is found due to the *p-d* hybrid orbitals of Co. Moreover, the optical features of the Co-doped BTO compound are evaluated by analyzing the refractive index, reflectivity, absorption coefficient, optical conductivity, and dielectric constant under different concentrations. The outcomes revealed that the $BaTi_{1-x}Co_xO_3$ compound is a good candidate for spintronics and optoelectronic applications.

(Received April 28, 2023; Accepted July 7, 2023)

Keywords: Optical properties, Semiconductors, Doping, DFT, Spintronics

1. Introduction

The constant efforts to explore significantly smaller information storage devices open up many areas of interest. In this context, spintronics is in limelight due to the usage of both the spin and charge of electrons to improve the information density. Dilute magnetic semiconductors (DMS) have been probed extensively owning to semiconducting and magnetic features and their need in spintronic and rotating electronic devices [1-3]. In modern research, there are various methods to fabricate DMSs by doping various elements, particularly ferromagnetic elements like Fe, Mn, V, Co, Cr, and Ni into non-ferromagnetic semiconductors [3-5]. Various materials like metal oxides, alloys, and perovskites demonstrate the DMSs behavior. However, perovskite oxides have received immense interest owning physical features like ferroelectricity, ionic conductivity, multiferroic, and superconductivity [6-8]. Their energy bands are anomalous and structures are different, however, have applications in various devices due to faster data delivery, low energy consumption, and high circuit integration density [9, 10].

Among them, the $BaTiO_3$ (barium titanate) is known to have a perovskite ferroelectric material. Recently, BTO attracted much attention from many researchers due to its abundant physical features like high dielectric constant and room temperature ferromagnetism [11, 12]. Due to its superb physical characteristics, it has been extensively studied experimentally and theoretically [13-15]. Nakayama and Katayama-Yoshida executed first-principles calculations for X-doped BTO (X= Mn, Sc, Cr, Cu, Co, Fe, Ni, V) within LDA and estimated that the Fe and Cr/Mn doped BTO are good contenders for production of the ferromagnetism [16]. In another study, ferromagnetism was introduced in the pure $BaTiO_3$ by introducing Co and Fe elements at

* Corresponding author: m.yaseen@uaf.edu.pk
https://doi.org/10.15251/CL.2023.207.459

the A site [17]. Recently, Lee *et al*. stated that the doping of TM= Co, Mn in BTO/STO and $KTaO_3$ compounds could induce magnetic behavior at room temperature [18]. Teng *et al.* explored the BS and optical characteristics of N/B or C-doped BTO using *ab-initio* calculations [19]. In addition, Cao *et al*. theoretically computed the electronic and magnetic features of Co-doped BTO by DFT and predicted a magnetic moment per Co atom of 3.15 μB [20].

Herein, we performed computation based on the DFT to predict the optical, magnetic, and electronic characteristics of cobalt-doped $BaTiO_3$. Our paramount goal is to evaluate the magnetism at different concentrations of Ba doping (8.33 %, 16.66%, 25%, and 50%), and to express their prospective applications in spintronic and optical devices.

2. Method of calculation

The theoretical calculations in this work are performed by using the FP-LAPW method as implemented into WIEN2k code within the framework of DFT [21]. The exchange-correlation interactions are computed by Generalized gradient approximation (GGA) [22, 23]. The Ba ($6s^2$), Co ($4d^{10}5s^2$), Ti ($3d^24s^2$), and O ($2s^22p^4$) are considered valance electrons. Inside a muffin-tin sphere, the crystal wave function and potential are expended based on spherical harmonic function whereas the plane wave solutions are selected for the interstitial region. The values of muffin tin radii (R_{MT}) are taken to be 2.68, 2.15, and 1.52 (bohr) for Ba, Ti, O, and Co atoms, respectively. The wave function i.e. l_{max}= 10 inside the sphere and the convergence parameter R_{MT} x K_{MAX} is set to be 10 to control the plane wave expansion. The Brillouin zone integration is performed using 1000 k-points which is based on the mesh of 10x10x10. A supercell of 3×2×2 was chosen for the doping of Co in the BTO structure. A schematic diagram of crystal structures for $BaCo_xTi_{1-x}O_3$ is shown in Fig. 1. The value of G_{max} is selected as 14 and the energy cut-off parameter is -6.0 Ry to evade the leakage of the charge[24].

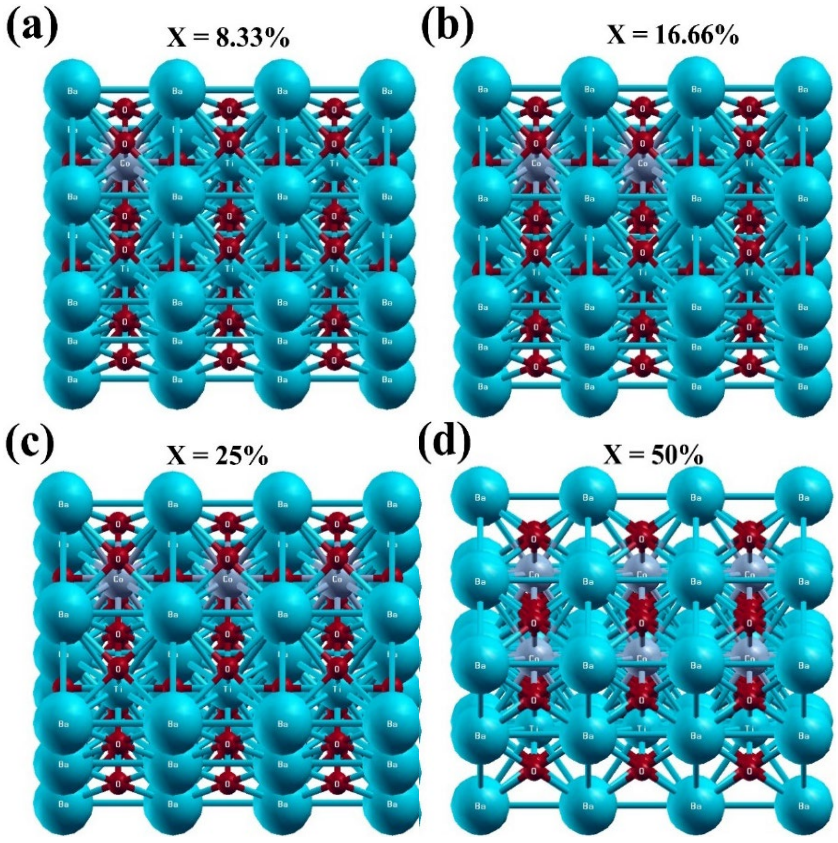

Fig. 1. Schematic crystal structures of $BaCo_xTi_{1-x}O_3$.

3. Results and discussions

3.1. Electronic properties

The electronic features including the density of states (DOS) and band structure (BS) of $Ba_{1-x}Co_xTiO_3$ (x= 8.33%, 16.66%, 25%, and 50%) compounds have been studied by employing GGA method as shown in Fig. (2-5). The pure BTO has a E_g of 1.83 eV [25]. Fig. 2(a-d) depicts the spin-polarized electronic BS of the BTO perovskites at different concentrations of Co doping, along the high symmetry direction of the Brillouin zone. It is observed that the spin-dependent outcomes show the high splitting among spin up/down states near the Fermi region. The spin-up/down states of the Co-doped BTO compound preserve the semiconductor behavior. However, the calculated band-gaps (see Fig. 2a, b) for $Ba_{1-x}Co_xTiO_3$ at x= 8.33% and 16.66% are 1.67, 1.64 eV in the spin-up and 1.69, 1.56 eV in spin-down versions, correspondingly. For x= 25% and 50%, the values of the E_g are 1.73 and 1.71 eV for spin up version (see Fig. 2(c, d)) whereas 1.64 and 1.54 eV for the spin-down version, respectively.

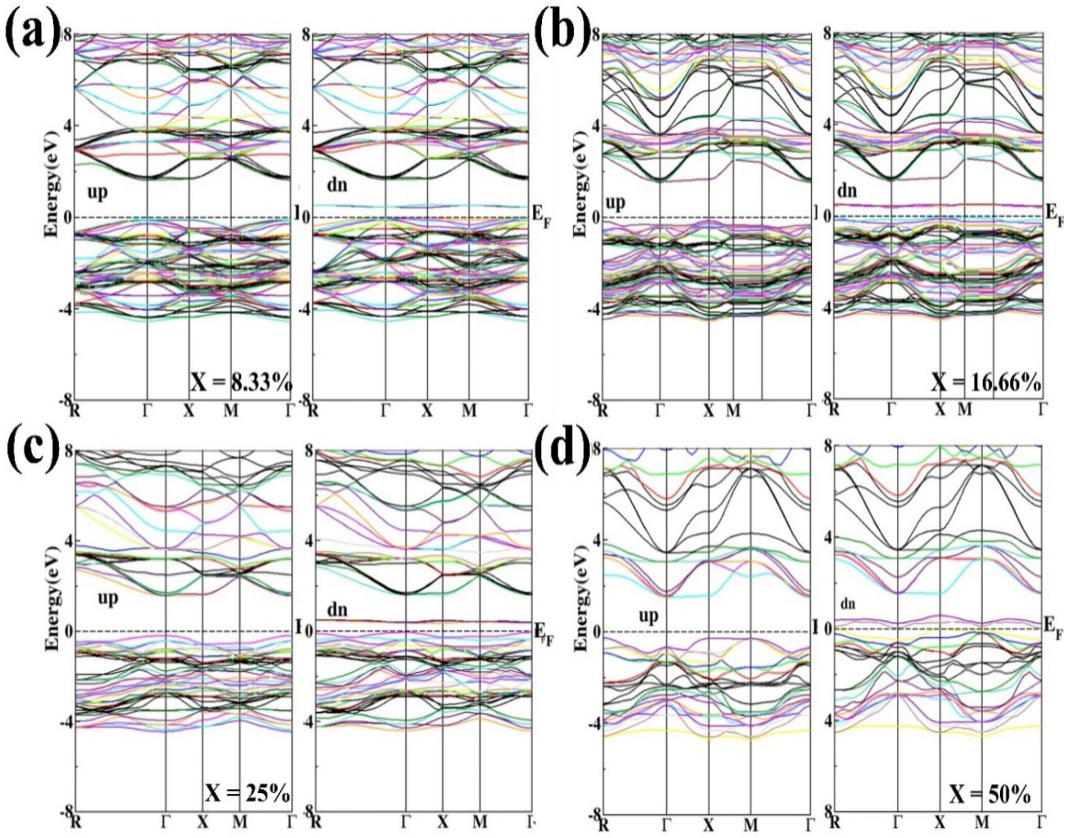

Fig. 2. Electronic BS of $BaCo_xTi_{1-x}O_3$.

For the clarification of BSs, the total DOS and partial DOS are computed. The calculated TDOS and PDOS for $BaTi_{1-x}Co_xO_3$ at x= 8.33%, 16.66%, 25%, and 50% are plotted in Figs. 3-5. The TDOS (Figs. 3 and 4) illustrate the same semiconducting nature of $BaTi_{1-x}Co_x$ as the band structure which enhances the reliability of the presented outcomes. The PDOS is plotted for Ba-*s,p*, Ti-*d*, O-*p,* and Co-*d* states, to explain the involvement of individual orbitals in total-DOS as shown in Fig. 5. The contribution of Co-*d* is most important owning to partially filled states. In all concentrations, the orbital behavior of the conduction band (CB) is majorly consisted of O-*p* orbital. In $BaTi_{1-x}Co_x$ (x= 8.33%), the contribution of Co-*d* is large in the valance band (VB) region than the other states of elements. Moreover, the CB ranges from 1.6-8 eV and is mainly composed of O-*p* orbital with a prominent peak at 3.3 eV in both spin versions arising due to the Ti-*d* state. The hybridization exists among the Ba-*s/p* and Ti-*d* states from –0.4 to -3.7 eV.

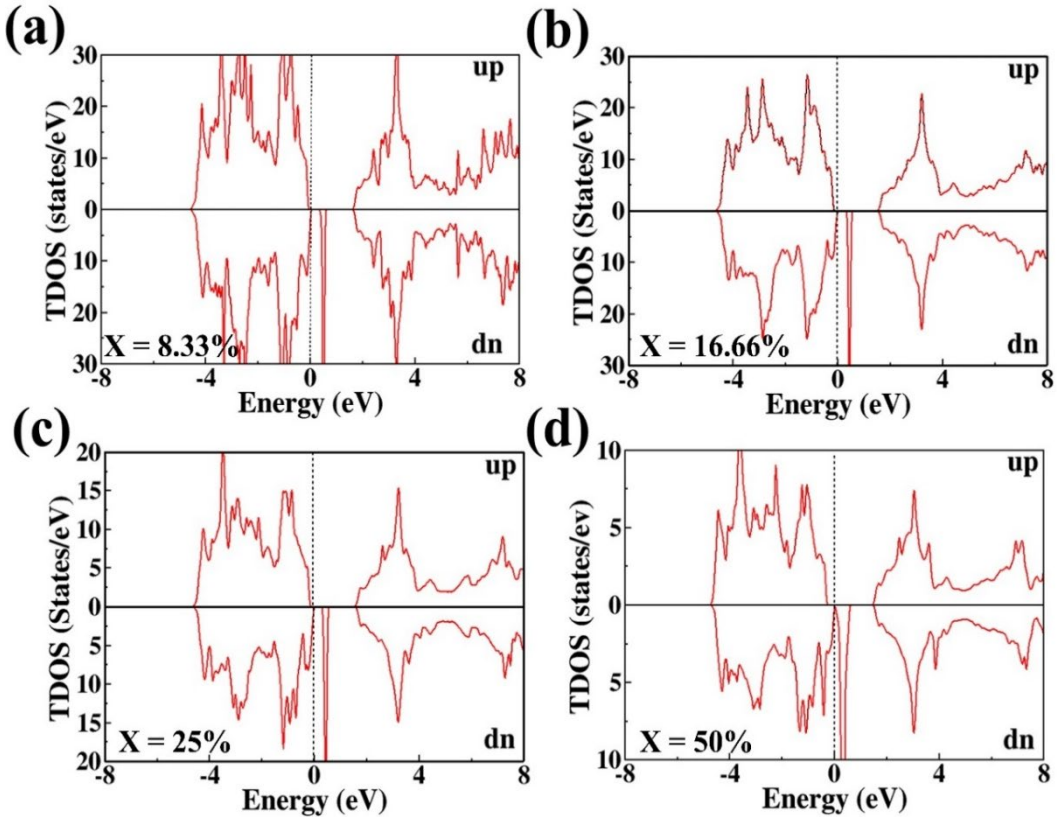

Fig. 3. Spin-dependent TDOS of $BaCo_xTi_{1-x}O_3$.

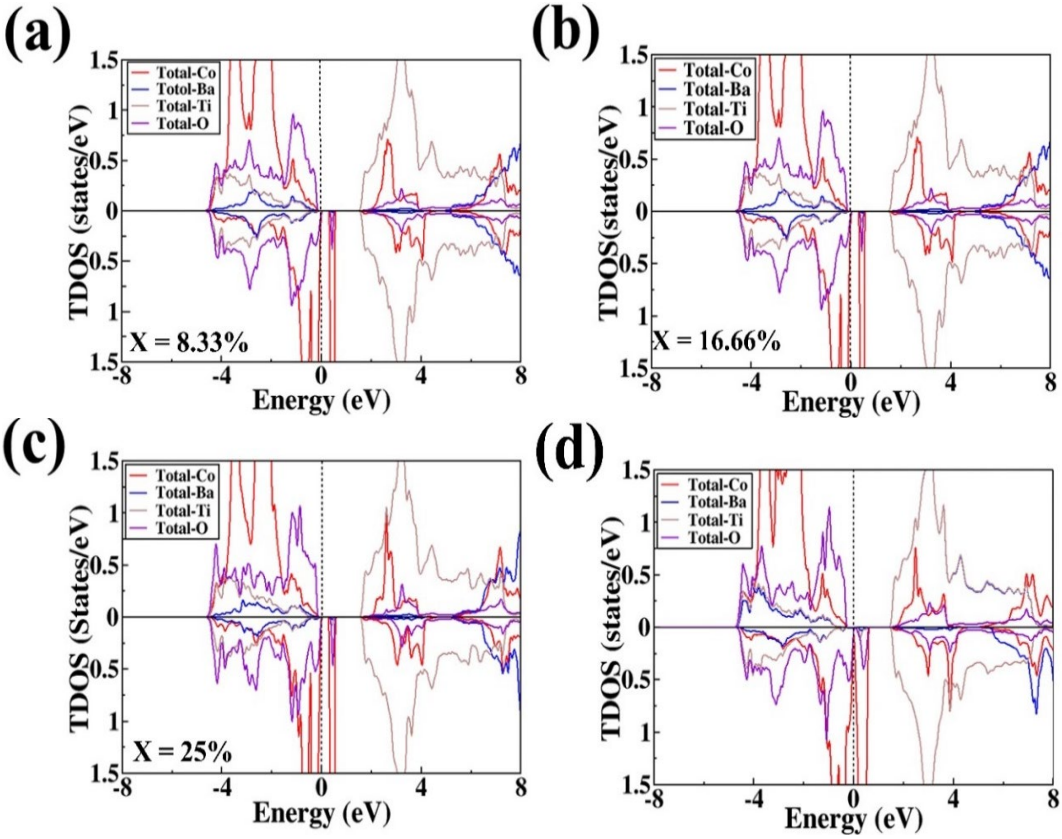

Fig. 4. Spin-dependent TDOS of $BaCo_xTi_{1-x}O_3$.

For x= 16.66%, 25%, and 50%, the VB is majorly dominated by Co-*d* and O-*p* states with small addition of Ti-*d* and Ba-*s/p* states. While for both spin configurations, the CB belongs to the Ti-*d* state (from 1.5-8 eV) with a feeble role of the O-*p* state (see Fig. 5b, c, d). The *p*-state of O atom and *d*-state of Co exhibit the highest role around E_F. From Fig. 5(b-d), it is observed that strong hybridization occurs among the *p* state of the oxygen atom and the Co-*d* state around the Fermi region in the spin-down channel.

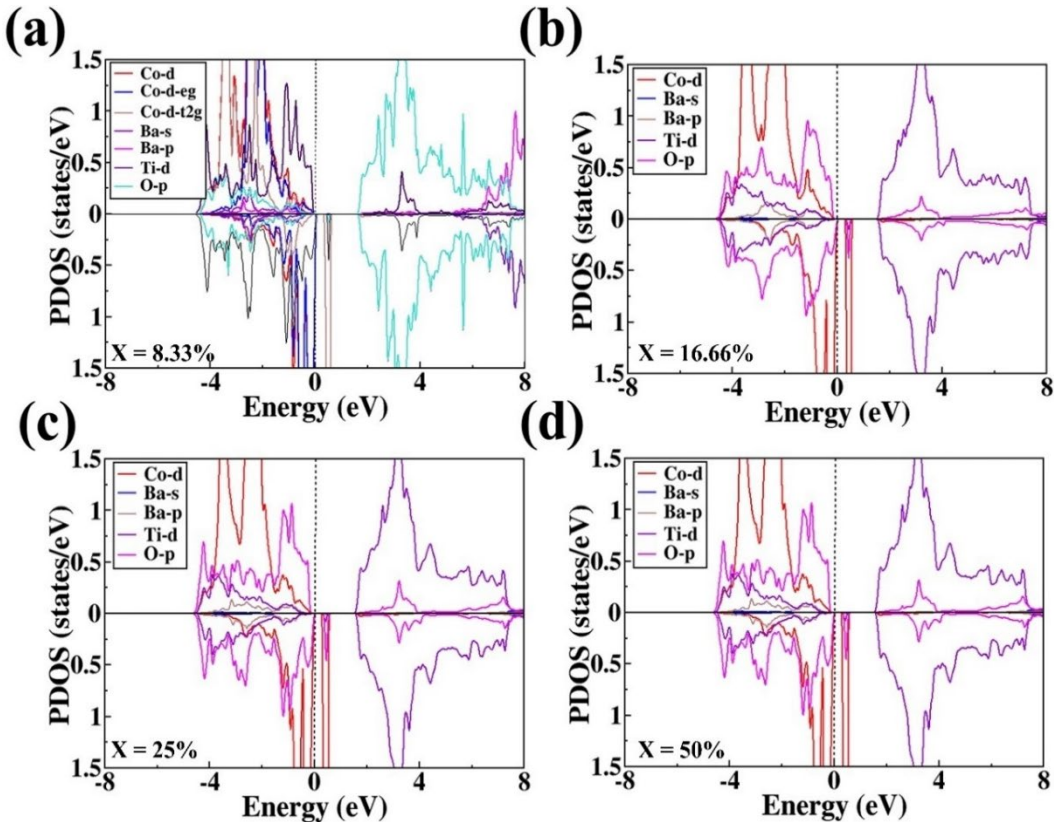

Fig. 5. Spin-dependent PDOS of $BaCo_xTi_{1-x}O_3$.

3.2. Optical properties

The optical features play an essential contribution to the interior structure of any material. The optical parameters of $Ba_{1-x}Co_xTiO_3$ (x= 8.33 %, 16.66 %, 25%, and 50%) have been investigated in terms of conduction, absorption, reflection, polarization, and dispersion. The optical behavior of any material can be analyzed by complex dielectric constants $\varepsilon(\omega)$, consisting of $\varepsilon_1(\omega)$ and part $\varepsilon_2(\omega)$. The real part shows the dispersion of light after interaction with the material's surface while the $\varepsilon_2(\omega)$ indicates the absorption $\alpha(\omega)$ of incident radiation. $\varepsilon_1(\omega)$ and $\varepsilon_2(\omega)$ are related through the Kramer-Kroning relation [26]. The value of the real part for Co-doped $BaTiO_3$ at 8.33%, 16.66%, 25%, and 50% concentrations are 7.8, 7.9, 8.5, and 12, respectively. The maximum peak appears at 0.4 eV for 50% doping. After some energy span, it starts reducing (see Fig. 6a) and then becomes zero.

Moreover, the band gap of the probed material at all concentrations and the static value $\varepsilon_1(0)$, formulated in form of Penn's model [20] is symbolized as $\varepsilon_1(0) = 1+(\hbar\omega_p/E_g)^2$. At all concentrations, the values of the imaginary part are zero at 0 eV, which means that there is no dissipation of energy within the system. The $\alpha(\omega)$ of light has top value at the maximum curve of the $\varepsilon_2(\omega)$ and dispersion of the light is low. According to Fig. 6(b), the $\varepsilon_2(\omega)$ exhibits maximum absorption at 4.1 eV, verifies the material's capability for optoelectronic devices, and then uniformly decrements with elevation of energy. The $n(\omega)$ and $k(\omega)$ has a similar pattern as real and imaginary parts and mentioned quantities are linked through $n^2 - k^2 = \varepsilon_1(\omega)$ and $2nk = \varepsilon_2(\omega)$

[27]. Similar to the imaginary part the k (ω) is also linked with α (ω) of light. Fig. 6c revealed the highest values of the k (ω) appear at 4.2 eV for all doping concentrations.

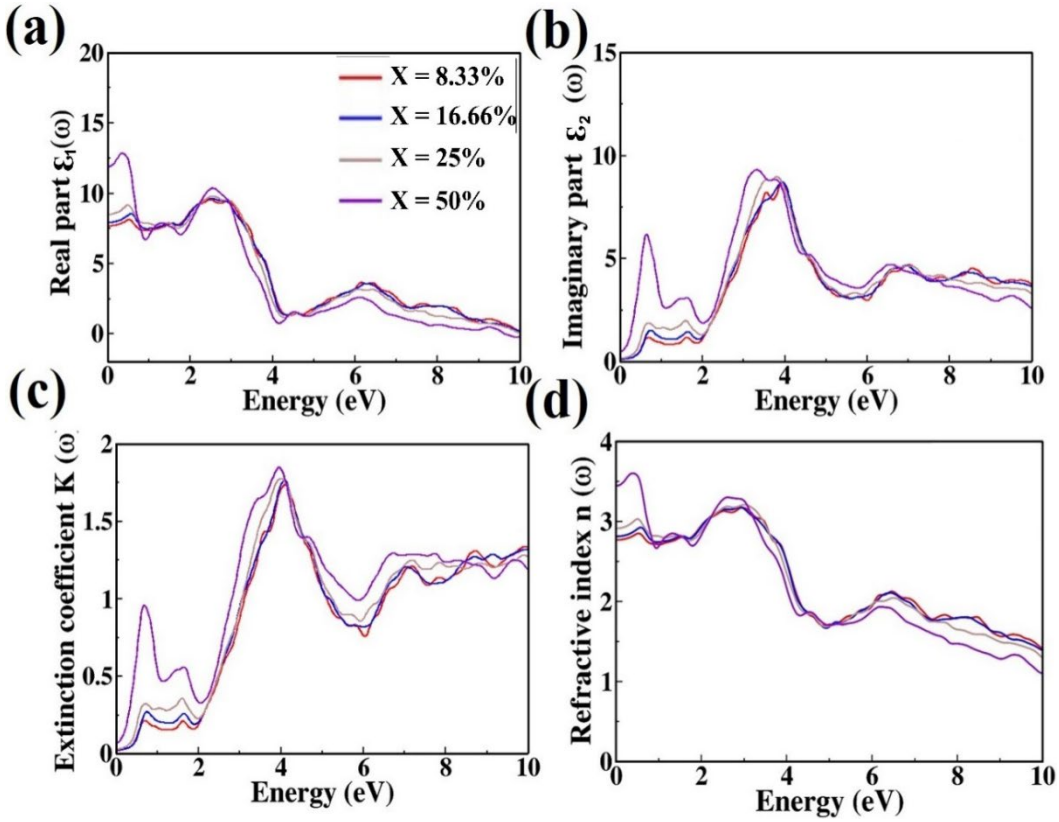

Fig. 6. (a) $\varepsilon_1(\omega)$, (b)$\varepsilon_2(\omega)$, (c) k (ω) and (d) n (ω) of $BaCo_xTi_{1-x}O_3$.

As the k (ω) increases the absorption coefficient also increases. The $n(\omega)$ shows the propagation of light within the material and it is essential phenomenon to study the optical feature of materials. The computed values of the $n(\omega)$ are 2.7, 2.8, 2.9, and 3.4 for 8.33%, 16.66%, 25%, and 50%, respectively (see Fig. 6d). For all concentrations, the maximum peak of $n(\omega)$ occurred at 3.1 eV then decreases in fluctuation form with increasing photon energy. The $k(\omega)$ and $n(\omega)$ are calculated by the following formula [28]

$$k(\omega) = \frac{\alpha\lambda}{4\pi} \tag{1}$$

$$n(\omega) = \left(\frac{\left[\varepsilon_1^2(\omega) + \varepsilon_2^2(\omega)\right]^{\frac{1}{2}}}{2}\right)^{1/2} \tag{2}$$

Furthermore, the $R(\omega)$ clarify the behavior of the material surface. At 50% doping, the dopant compound shows maximum reflectivity of 3.0 at zero photon energy. The maximum curves of the $R(\omega)$ emerges at 4.2 eV for all concentrations as depicted in Fig. 7a. The values of the $R(\omega)$ follow the same trend as the ε_1 (ω). The absorption is maximum at all points where the reflectivity is minimum. The α (ω) depends upon the frequency of the light absorbed in the substanc. The maximum α (ω) occurs at 4.1 eV for all doping concentrations which confirms that the studied material is optically active in visible to UV regions that are important for optoelectronic applications (See Fig. 7b). In addition, the σ (ω) defines the bond breaking in a material by incident light on material's surface. At different concentrations, the σ (ω) is elucidated in Fig. 7c. From Fig. 7 (b, c), it is found that the optical conductivity and α (ω) almost illustrate

similar behavior. At 5.8 eV the value of the *α (ω)* and the *σ (ω)* is minimum and then slightly increases with increasing the value of energy.

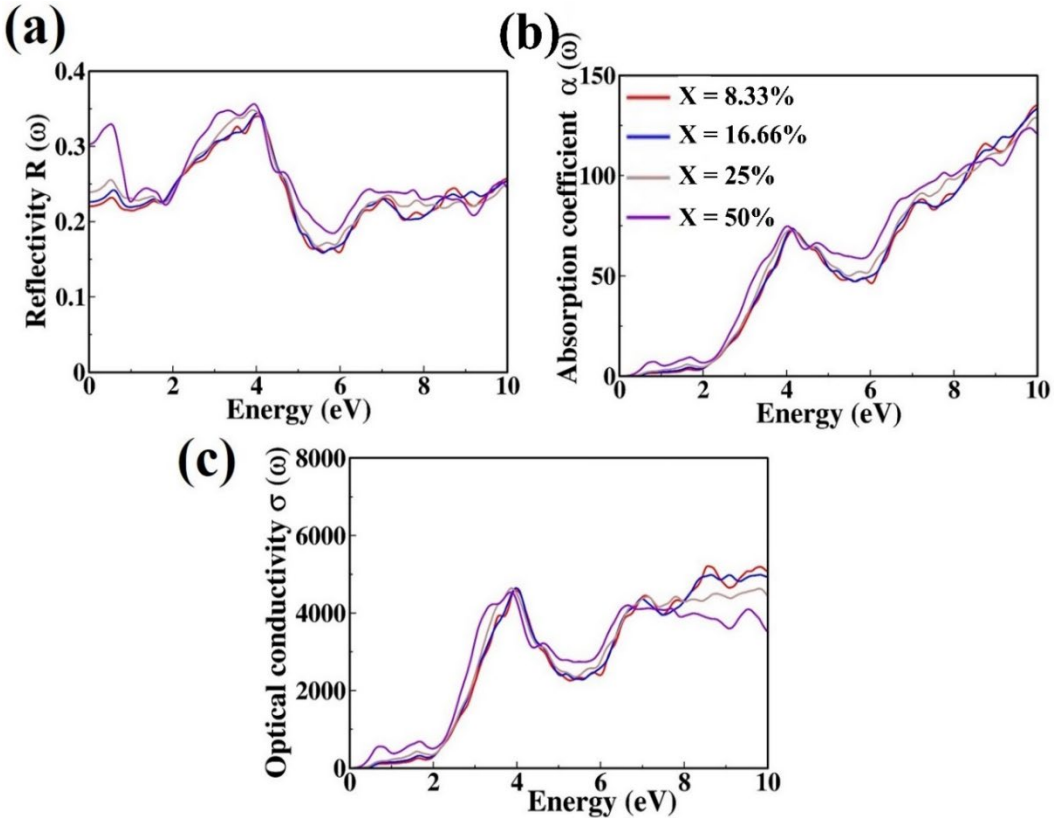

Fig. 7. (a) R (ω), (b) α (ω) and (c) σ (ω) of $BaCo_xTi_{1-x}O_3$.

3.3. Magnetic properties

In the $Ba_{1-x}Co_xTiO_3$ compound, the total magnetic moments (μB), interstitial magnetic moments, as well as atomic magnetic moments of Ba, Ti, O, and Co atoms at different Co doping are computed (see Table 1). It is observed that the M_{tot} of $Ba_{1-x}Co_xTiO_3$ at x= 8.33%, 16.66%, 25%, and 50% are 3.000, 3.002, 2.999, and 3.000 μB, respectively.

Table 1. Computed M_{TOT} per Co atom (μB), interstitial magnetic moments and atomic magnetic moment of each site for $BaTi_{1-x}Co_xO_3$.

Concentration	Magnetic Moment (μB)					
	Total	Interstitial	Co	Ba	Ti	O
X= 8.33%	3.00009	0.04148	2.62968	0.0011	0.00006	0.02653
X= 16.66%	3.00278	0.04041	2.63470	0.00234	- 0.00423	0.14036
X= 25%	2.99992	0.04117	2.63449	0.00268	-0.00356	0.08367
X= 50%	3.00004	0.03869	2.62816	0.00284	-0.00812	0.17664

The obtained values show that the M_{Tot} mainly originated from the Co atom with a small contribution of Ba, Ti, and oxygen atoms. The unfilled Co-*d* states cause the production of the atomic magnetic moment due to *p-d* hybridization among Co-*d* and O-*p* states whereas small magnetism originates from feeble hybridization among non-magnetic Ba-*s/p* and Ti-*d* states. Besides, it is found that the magnetic moments for Ba, O, and Co are in positive signs referring to

parallel spin while the negative value for Ti suggests the anti-parallel alignment of the magnetic moment.

4. Conclusions

In this research, the electronic, optical, and magnetic properties of the $BaTi_{1-x}Co_xO_3$ (x= 8.33%, 16.66%, 25%, and 50%) compounds have been studied by using the FP-LAPW approach within DFT. The analysis of BS and DOS in both spin versions exhibits the semiconductor behavior at different concentrations. The outcomes show that the magnetic moment (μB) primarily comes from the Co-*d* orbital. In addition, the total μB is found about 3.00 μB per Co-atom for $BaTi_{1-x}Co_xO_3$ (x= 8.33%, 16.66%, 25%, and 50%). The variation in different optical parameters with doping is also examined. The large absorption in the visible to UV portion of the electromagnetic (EM) spectrum favors investigated material for optoelectronic and spintronic devices.

Acknowledgement

The authors express their gratitude to Princess Nourah bint Abdulrahman University Researchers Supporting Project number (PNURSP2023R55), Princess Nourah bint Abdulrahman University, Riyadh, Saudi Arabia.

References

[1] Ohno, H., Chiba, A.D., Matsukura, A.F., Omiya, T., Abe, E., Dietl, T., Ohno, Y. and Ohtani, K., Nature. 408(6815) 944-946 (2000); https://doi.org/10.1038/35050040

[2] R. Masrour, E. K. Hlil, M. Hamedoun, A. Benyoussef, A. Boutahar, H. Lassri, Journal of Magnetism and Magnetic Materials 393, 600-603 (2015); https://doi.org/10.1016/j.jmmm.2015.05.085

[3] Hamedoun, M., Elachheb, Z., Bakrim, H., Hourmatallah, A., Benzakour, N., Jorio, A. and Hachimi, M., Physica Status Solidi B 236(3), 661-667 (2003); https://doi.org/10.1002/pssb.200301653

[4] Sharma, V.K., Xalxo, R. and Varma, G.D., Journal of Experimental and Industrial Crystallography, 42(1), 34-38 (2007); https://doi.org/10.1002/crat.200610766

[5] Furdyna, J.K. and Samarth, N., Journal of Applied Physics, 61(8), 3526-3531 (1987); https://doi.org/10.1063/1.338714

[6] Saghi-Szabo, G., Cohen, R.E. and Krakauer, H., Physical Review Letters, 80(19), 4321 (1998); https://doi.org/10.1103/PhysRevLett.80.4321

[7] Ali, Z., Sattar, A., Asadabadi, S.J. and Ahmad, I., Journal of Physics and Chemistry of Solids, 86, 114-121 (2015); https://doi.org/10.1016/j.jpcs.2015.07.001

[8] Shimakawa, Y., Azuma, M. and Ichikawa, N., Materials, 4(1), 153-168 (2011); https://doi.org/10.3390/ma4010153

[9] Bouadjemi, B., Bentata, S., Abbad, A. and Benstaali, W., Solid State Communications, 207, 9-15 (2015); https://doi.org/10.1016/j.ssc.2015.02.001

[10] Yang, R., Li, R., Cao, Y., Wei, Y., Miao, Y., Tan, W.L., Jiao, X., Chen, H., Zhang, L., Chen, Q. and Zhang, H., Advanced Materials, 30(51), 1804771 (2018); https://doi.org/10.1002/adma.201804771

[11] Spanier, J.E., Kolpak, A.M., Urban, J.J., Grinberg, I., Ouyang, L., Yun, W.S., Rappe, A.M. and Park, H., Nano letters, 6(4), 735-739 (2006); https://doi.org/10.1021/nl052538e

[12] Ali, A., Khan, I., Ali, Z., Khan, F. and Ahmad, I., International Journal of Modern Physics B, 33(21), 1950231 (2019); https://doi.org/10.1142/S021797921950231X

[13] Yi, J.B., Lim, C.C., Xing, G.Z., Fan, H.M., Van, L.H., Huang, S.L., Yang, K.S., Huang, X.L., Qin, X.B., Wang, B.Y. and Wu, T., Physical review letters, 104(13), 137201 (2010); https://doi.org/10.1103/PhysRevLett.104.137201

[14] Tong, X., Lin, Y.H., Zhang, S., Wang, Y. and Nan, C.W., Journal of Applied Physics 104, 066108 (2008); https://doi.org/10.1063/1.2973202

[15] Kumbhar, S.S., Mahadik, M.A., Chougule, P.K., Mohite, V.S., Hunge, Y.M., Rajpure, K.Y., Moholkar, A.V. and Bhosale, C.H., Materials Science-Poland, 33(4), 852-861 (2015); https://doi.org/10.1515/msp-2015-0107

[16] Nakayama, H.N.H. and Katayama-Yoshida, H.K.Y.H., Japanese journal of applied physics, 40(12B), L1355 (2001); https://doi.org/10.1143/JJAP.40.L1355

[17] Yang, L., Qiu, H., Pan, L., Guo, Z., Xu, M., Yin, J. and Zhao, X., Journal of magnetism and magnetic materials, 350, 1-5 (2014); https://doi.org/10.1016/j.jmmm.2013.09.036

[18] Lee, J.S., Khim, Z.G., Park, Y.D., Norton, D.P., Theodoropoulou, N.A., Hebard, A.F., Budai, J.D., Boatner, L.A., Pearton, S.J. and Wilson, R.G., Solid-State Electronics, 47(12), 2225-2230 (2003); https://doi.org/10.1016/S0038-1101(03)00202-8

[19] Teng, Z., Jiang, J., Chen, G., Ma, C. and Zhang, F., AIP Advances, 8(9), 095216 (2018); https://doi.org/10.1063/1.5047094

[20] Cao, D., Liu, B., Yu, H., Hu, W. and Cai, M., The European Physical Journal B, 88, 1-7 (2015); https://doi.org/10.1140/epjb/e2015-50491-1

[21] Blaha, P., Schwarz, K., Sorantin, P. and Trickey, S.B., Computer physics communications, 59(2), 399-415 (1990); https://doi.org/10.1016/0010-4655(90)90187-6

[22] A. Sohail, S. A. Aldaghfag, M. K. Butt, M. Zahid, M. Yaseen, J. Iqbal, Misbah, M. Ishfaq, A. Dahshan, Journal of Ovonic Research, 17(5), 461-469 (2021).

[23] Blöchl, P.E., Physical review B, 50(24), 17953 (1994); https://doi.org/10.1103/PhysRevB.50.17953

[24] M.Yaseen, A.Ashfaq,A.Akhtar,R. Asghar, H.Ambreen, M. K.Butt, A. Murtaza, Materials Research Express, 7(1), 015907(2020); https://doi.org/10.1088/2053-1591/ab6110

[25] Naz, A., Aldaghfag, S.A., Yaseen, M., Butt, M.K., Kashif, M., Zahid, M., Mubashir, S. and Somaily, H.H., Physica B: Condensed Matter, 631, 413714 (2022); https://doi.org/10.1016/j.physb.2022.413714

[26] Marius, G., The physics of semiconductors: Kramers-Kronig relations. 2010, Springer, Berlin Heidelberg.

[27] Butt, M.K., Yaseen, M., Bhatti, I.A., Iqbal, J., Murtaza, A., Iqbal, M., mana AL-Anazy, M., Alhossainy, M.H. and Laref, A., Journal of Materials Research and Technology, 9(6), 16488-16496 (2020); https://doi.org/10.1016/j.jmrt.2020.11.055

[28] Butt, M.K., Yaseen, M., Ghaffar, A. and Zahid, M., Arabian Journal for Science and Engineering, 45, 4967-4974 (2020); https://doi.org/10.1007/s13369-020-04576-6